Photophysics and Bonding in Neutral Gold(I) Organometallic Complexes with an Extended Aurophilic Supramolecular Structure

Oussama Elbjeirami,[†] Scott Yockel,[†] Charles F. Campana,[‡] Angela K. Wilson,*[,†] and Mohammad A. Omary*[,†]

Department of Chemistry and Center for Advanced Scientific Computing and Modeling (CASCaM), University of North Texas, P.O. Box 305070, Denton, Texas 76203-5070, and Bruker AXS Inc., 5465 East Cheryl Parkway, Madison, Wisconsin 53711-5373

Received June 15, 2006

This work represents a synergistic experimental/computational study of the molecular spectroscopy and bonding in Au(CO)Cl in solution and the solid state. The luminescence behavior for crystalline solids is similar for Au(CO)Cl and related (RNC)AuCl complexes that likewise stack in infinite chains, and both exhibit orange-red unstructured phosphorescence bands with extremely large Stokes shifts ((15−20) × 10^3 cm^{-1}). The long aurophilic distances computed for the ground state (∼3.2 Å) are contracted in the phosphorescent excited state (∼2.6 Å), demonstrating excimeric Au−Au covalent bonds. The spectral data suggest phosphorescent species in which the excimeric Au−Au bonding is extended beyond two adjacent molecules in the solid state. Controlling the concentration in frozen solutions attains phosphorescent bands due to dimeric species for which the emission energies are higher (in the blue region) than those for crystalline solids and are reproduced by ab initio calculations. The spectral findings herein suggest that predictive information about the supramolecular structure may be obtained by the luminescnce behavior. This is exemplified by crystals of (1,1,3,3-Me_4BuNC)AuCl, whose red-orange luminsecence anticipated an extended-chain supramolecular structure, which was later verified crystallographically, as the molecules were found to pack in zigzag chains with alternating short (3.418 Å) and long (4.433 Å) aurophilic distances. Solutions of Au(CO)Cl exhibit negative deviation from Beer's law for, higher-energy monomer bands with the appearance of lower-energy bands at high concentrations due to the dimerization of molecules. Time-dependent density-functional theory (TD-DFT) calculations for monomer and dimer models show good agreement with the experimental spectra and account for the major absorption bands. Ab initio calculations (CCSD(T)/cc-pVTZ) show a blue shift of ∼23 cm^{-1} in the $\nu_{C\equiv O}$ frequency upon complexation, thus providing the first computational evidence of this anomalous blue shift known experimentally for Au(CO)Cl.

Introduction

Chlorocarbonylgold(I) was first prepared in 1925[1] and has been used as a common starting material for Au^I complexes, since the carbonyl species can be readily displaced by other ligands. This compound is extremely air and moisture sensitive and forms a colorless crystalline solid.[1] The crystal structure of Au(CO)Cl reveals that the molecules are arranged in head-to-tail antiparallel infinite chains with Au···Au contacts of 3.38 Å,[2] similar to their isoelectronic RNCAu^ICl neutral isonitrile compounds, that have identical association of antiparallel chains.[3] The stability of the halogen carbonyl complexes of Au(I) follows the same trend established earlier for palladium(II) and platinum(II), with the stability for all these complexes decreasing along the sequence Cl > Br > I.[4,5] One interesting IR characteristic in the Au(CO)Cl complex is the high $\nu_{C\equiv O}$ stretching vibrational frequency (2152−2162 cm^{-1} with some solvent dependence), which has been attributed to only modest π back-donation from the metal to the carbonyl group.[6] Calderazzo and co-workers reported a seminal study on the properties of Au(CO)X compounds, in which they surveyed a number of ligands.[7] In addition to gold, other d^{10} metal−carbonyl complexes have been studied to a lesser extent. For example, copper carbonyl species of the form Cu^I(CO)X (X = Cl, Br, CF_3COO) have been isolated or at least identified, while structurally characterized carbonyl complexes of silver(I) are rare and harder to isolate.[8−15] It is clear from experimental evidence that gold carbonyl species are the most stable thermodynamically, in comparison to the analogous copper and silver complexes, with an Au−CO bond energy of ∼200 kJ/mol as estimated by Calderazzo.[7]

* To whom correspondence should be addressed. E-mail: omary@unt.edu (M.A.O.); akwilson@unt.edu (A.K.W.).
† University of North Texas.
‡ Bruker AXS Inc.

(1) Manchot, W.; Gall, H. *Ber. Bunsen-Ges. Phys. Chem.* **1925**, *58*, 2175.
(2) Jones, P. G. *Z. Naturforsch., B* **1982**, *37*, 823.
(3) White-Morris, R. L.; Olmstead, M. M.; Balch, A. L.; Elbjeirami, O.; Omary, M. A. *Inorg. Chem.* **2003**, *42*, 6741.
(4) Andreini, B. P.; DellAmico, D. B.; Calderazzo, F.; Venturi, M. G.; Peizzi, G.; Serge, A. *J. Organomet. Chem.* **1988**, *354*, 357.
(5) DellAmico, D. B.; Calderazzo, F.; Robino, P.; Serge, A. *J. Chem. Soc., Dalton Trans.* **1991**, *3*, 3017.
(6) DellAmico, D. B.; Calderazzo, F. *Gazz. Chim. Ital.* **1973**, *103*, 1099.
(7) Calderazzo, F. *J. Organomet. Chem.* **1990**, *400*, 303.
(8) Meyer. R. J.; Pietsch, E. H.; Kotowski, A. *Gmelin Handbuch der Anorganischchen Chemie*; Springer: Berlin, 1975; Silver Part B5.
(9) Antes, I.; Dapprich, S.; Frenking, G.; Schwerdtfeger, P. *Inorg. Chem.* **1996**, *35*, 2089.
(10) Caulton, K. G.; Davies, G.; Holt, E. M. *Polyhedron* **1990**, *9*, 2319.
(11) Bruce, M. I.; Ostazewski, A. P. P. *J. Chem. Soc., Dalton Trans.* **1973**, 2433.
(12) Dias, H. V. R.; Lu, H. L. *Inorg. Chem.* **1995**, *34*, 5380.
(13) Dias, H. V. R.; Jin, W. *J. Am. Chem. Soc.* **1995**, *117*, 11381.
(14) Hurlburt, P. K.; Rack, J. J.; Dec, S. F.; Anderson, O. P.; Strauss, S. H. *Inorg. Chem.* **1993**, *32*, 373.
(15) Dias, H. V. R.; Wiechang, J. *Inorg. Chem.* **1996**, *35*, 3687.

10.1021/om060524t CCC: $37.00
Publication on Web 03/31/2007

The organometallic literature suggests that metal isonitriles have been strongly overshadowed by metal carbonyls, most likely because of the repulsive smell of isonitriles and not essentially due to scientific reasons. The electronic structure of RNC has been shown to be rather similar to that of CO;[16] thus, similar reactivity is expected for analogous complexes of both ligands. The chemistry of metal isonitriles is relevant to several interesting applications. For example, gold(I) isonitrile complexes have been utilized for the deposition of gold films[17,18] and for the preparation of new types of liquid crystalline phases.[19,20] The versatility enabled by varying the R group in RNC ligands makes them good candidates to contribute to the current state of knowledge regarding the photochemistry and photophysics of Cu^I, Ag^I, and Au^I species.[21,22]

The present study investigates the spectral and bonding properties for solids of both Au(CO)Cl and (RNC)AuCl species, which have similar solid-state packing. Detailed studies of the excited-state properties of carbonyl complexes of d^{10} metal ions are scarce.[23] When the excited-state properties of metal complexes are studied, it is found that an important distinction exists between d^{1-9} and d^{10} configurations, in that the electronic transitions with partially filled d subshells create ligand-field excited states, while these d−d transitions are absent in the closed-shell complexes. On the basis of this concept, the spectroscopy and photochemistry of such systems are reliant on the properties of other types of electronic excited states (e.g. ligand-to-metal charge transfer (LMCT) or metal-to-ligand charge transfer (MLCT)).[23] In 1997, the Vogler group reported a primarily photochemical study for Au(CO)Cl, with some preliminary photophysical results showing the compound to exhibit a longest-wavelength weak absorption feature at ∼250 nm.[24] They attributed this solution absorption to a metal-centered d−s transition, which the authors related to the solid-state emission band at λ_{max} 660 nm at room temperature.[24] Inspired by this precedent, herein we report a detailed spectroscopic and bonding characterization of Au(CO)Cl in the solid state and solution utilizing complementary experimental and computational methods to investigate this classical organometallic complex. In addition, we compare the properties of Au(CO)Cl to those of the closely related (RNC)AuCl (R = *tert*-butyl, methyl, cyclohexyl, and 1,1,3,3-tetramethylbutyl). We believe that this study contributes to a better understanding of the structure−luminescence relationships in mononuclear two-coordinate Au^I complexes. Despite the strong attention given to such complexes, a major challenge lies in trying to relate the luminescence energy or color to the crystallographic Au···Au ground-state distances.[25,26] Once this relationship is well-understood, it will be possible to design compounds to display specific luminescence properties, which can be used in single or multicolor electroluminescent display and solid-state light devices in which triplet emitters are significant.[27] We have recently communicated that the distinction for the Au-centered solid-state phosphorescence energy in such complexes is perhaps better drawn on the basis of the differences in the supramolecular structure instead of the shortest Au···Au distances, a hypothesis made after contrasting the photophysical properties of one compound in each category.[28] In an effort to assess the generality of this hypothesis, the present study examines the photophysical behavior of five LAuCl organometallic complexes (L = CO, RNC) that pack in infinite zigzag chains through aurophilic bonding.

Experimental and Computational Methodologies

Materials. Au(CO)Cl was purchased from Strem Chemicals, while cyclohexyl isocyanide (CyNC) and *tert*-butyl isocyanide (*t*-BuNC) were purchased from ACROS Organics. (THT)AuCl (THT = tetrahydrothiophene) and methyl isocyanide (MeNC) were synthesized by slight modifications of published procedures.[29,30] HPLC-grade acetonitrile and dichloromethane were distilled with conventional drying agents, degassed by the freeze−pump−thaw method three times prior to use, and kept under argon at all time. All absorption measurements were carried out under argon, and luminescence spectra were collected while the sample was kept under helium and in the dark unless otherwise indicated.

Syntheses. The preparation methods for (RNC)AuCl (R = cyclohexyl, methyl, *tert*-butyl) were reported previously[3,31,32] and were generally followed here for these compounds. Standard Schlenk line techniques under an argon atmosphere were followed in which equimolar amounts of (THT)AuCl and cyclohexyl isocyanide, methyl isocyanide, or *tert*-butyl isocyanide were dissolved in 10 mL of deaerated dichloromethane followed by stirring the solutions for 4 h. The solvent was then evaporated under reduced pressure, and a white solid formed, which was extracted with pentane, filtered, and dried under vacuum. Crystals were grown for each compound from CH_2Cl_2/pentane solutions of recrystallized solids.

(Me_4BuNC)AuCl (Me_4Bu = 1,1,3,3-Tetramethylbutyl). (THT)AuCl (200 mg, 0.62 mmol) was dissolved in 10 mL of deaerated dichloromethane. 1,1,3,3-Tetramethylbutyl isocyanide (122 μL, 0.70 mmol) was then added, and the solution was stirred for 4 h, after which the solvent was evaporated under reduced pressure and a white solid formed. The solid was washed several times with pentane, collected by filtration, and vacuum-dried (90% yield). Crystals were grown from a CH_2Cl_2/pentane solution of the recrystallized solid.

Physical Measurements. The luminescence measurements were carried out for crystalline materials. Steady-state luminescence spectra were acquired with a PTI QuantaMaster Model QM-4 scanning spectrofluorometer equipped with a 75 W xenon lamp, emission and excitation monochromators, an excitation correction unit, and a PMT detector. The emission and excitation spectra were corrected for the wavelength-dependent detector response and xenon lamp intensity, respectively. Temperature-dependent studies were acquired with an Oxford optical cryostat using liquid helium or liquid nitrogen as coolant. Lifetime data were acquired using a

(16) Elschenbroich, C.; Salzer, A. *Organometallics: A Concise Introduction*, 2nd ed.; VCH: Weinheim, Germany, 1992.
(17) Norton, P. R.; Young, P. A.; Cheng, Q.; Dryden, N.; Puddephatt, R. J. *Surf. Sci.* **1994**, *307*, 172.
(18) Vaughan, L. G.; U.S. Patent 3661959-19720509, 1972.
(19) (a) Bachman, R. E.; Fioritto, M. S.; Fetics, S. K.; Cocker, T. M. *J. Am. Chem. Soc.* **2001**, *123*, 537. (b) Kaharu, T.; Ishii, R.; Takahashi, S. *J. Chem. Soc., Chem. Commun.* **1994**, 1349.
(20) Ishi, R.; Kaharu, T.; Pirio, N.; Zhang, S. W.; Takahashi, S. *J. Chem. Soc., Chem. Commun.* **1995**, 1215.
(21) (a) Kual, C. *Coord. Chem. Rev.* **1990**, *99*, 213. (b) Ford, P. C.; Vogler, A. *Acc. Chem. Res.* **1993**, *26*, 220. (c) Hong, T. S.; Li, P.; Leong, W. K.; Fan, W. Y. *J. Organomet. Chem.* **2005**, *690*, 4132.
(22) Timney, J. A. *Organomet. Chem.* **1999**, *27*, 132.
(23) Shao, L.; Zhang, L.; Zhou, M.; Qin, Q. *Organometallics* **2001**, *20*, 1173.
(24) Kunkely, H.; Vogler, A. *J. Organomet. Chem.* **1997**, *541*, 177.
(25) Forward, J. M.; Fackler, J. P., Jr.; Assefa, Z. Photophysical and Photochemical Properties of Gold(I) Complexes. In *Optoelectronic Properties of Inorganic Compounds*; Roundhill, D. M., Fackler, J. P., Jr., Eds.; Plenum: New York, 1999; Chapter 6.
(26) Yam, V. W.; Lee, W. K. *J. Chem. Soc., Dalton Trans.* **1993**, 2097.
(27) Review: Yersin, H. *Top. Curr. Chem.* **2004**, *241*, 1.
(28) Elbjeirami, O.; Omary, M. A.; Stender, M.; Balch, A. L. *Dalton Trans.* **2004**, 3173.
(29) Usón, R.; Laguna, A. In *Organometallic Syntheses*; King, R. B., Eisch, J. J., Eds.; Elsevier: Amsterdam, 1986; Chapter 3.
(30) Schuster, R. E.; Scott, J. E.; Cazanova, J. *Org. Synth.* **1966**, *46*, 75.
(31) Eggleston, D. S.; Chodosh, D. F.; Webb, R. L.; Davis, L. L. *Acta Crystallogr., Sect. C* **1986**, *42*, 36.
(32) Schneider, W.; Angermaier, K.; Sladek, A.; Schmidbaur, H. *Z. Naturforsch., B* **1996**, *51*, 790.

nitrogen laser interfaced with a tunable dye laser and a frequency doubler, as part of fluorescence and phosphorescence subsystem add-ons to the PTI instrument. The 337.1 nm line of the N_2 laser was used to pump a freshly prepared 1×10^{-2} M solution of the organic continuum laser dye Coumarin-540A in ethanol, the output of which was tuned and frequency-doubled to attain the suitable excitation wavelength (on the basis of the steady-state luminescence excitation spectra) used to generate the time-resolved data. Absorption spectra were acquired with a Perkin-Elmer Lambda 900 double-beam UV/vis/near-IR spectrophotometer. Luminescence and lifetime studies for frozen solutions were conducted for selected samples by placing a 5 mm Suprasil quartz cylindrical tube containing the appropriate degassed solution in a liquid-nitrogen filled Dewar flask with a Suprasil quartz cold finger and then inserting this setup in the sample compartment of the PTI instrument. Electronic absorption spectra were collected using 1 cm quartz cuvettes for solutions of crystalline samples prepared in HPLC-grade acetonitrile that was degassed and kept under argon. Due to the sensitivity of the Au(CO)Cl compound, all manipulations and experiments for this compound were carried out in the dark and under an inert atmosphere.

Crystallographic Details. A clear, colorless, platelike specimen of $[(CH_3)_3CCH_2C(CH_3)_2NC]AuCl$, $C_9H_{17}NClAu$, approximate dimensions 0.10 mm × 0.36 mm × 0.44 mm, was used for the X-ray crystallographic analysis. The X-ray intensity data were measured at 100(2) K on a Bruker KAPPA APEX II CCD area detector system equipped with a graphite monochromator and a Mo Kα fine-focus sealed tube ($\lambda = 0.710\ 73$ Å) operated at 1.5 kW power (50 kV, 30 mA) and a Bruker Kryo-Flex low-temperature device. All data collection and structure determination operations were carried out with the APEX2 (version 2.0-2) Software Suite.[33] The detector was placed at a distance of 4.980 cm from the crystal. A total of 1435 frames were collected with a scan width of 0.5° in ω or ϕ and an exposure time of 30.0 s/frame. The total data collection time was 12.76 h. The frames were integrated with the Bruker SAINT[33] (version 3.23A) software package using a narrow-frame integration algorithm. The integration of the data using a monoclinic unit cell yielded a total of 20 025 reflections to a maximum θ angle of 30.60° (0.70 Å resolution), of which 3620 were independent (average redundancy 5.53, completeness 99.2%, $R_{int} = 3.14\%$, $R_{sig} = 2.07\%$) and 3177 (87.76%) were greater than $2\sigma(I)$. The final cell constants of $a = 19.9362(9)$ Å, $b = 8.0691(4)$ Å, $c = 14.8652(7)$ Å, $\beta = 98.263(2)°$, and $V = 2366.50(19)$ Å^3 are based upon the refinement of the *XYZ* centroids of 6915 reflections above $20\sigma(I)$ with $5.292° < 2\theta < 60.993°$. Analysis of the data showed negligible decay during data collection. Data were corrected for absorption effects using the multiscan technique (SADABS,[33] version 2.05). The ratio of minimum to maximum apparent transmission was 0.6655. The calculated minimum and maximum transmission coefficients (based on crystal size) were 0.0721 and 0.3652. The structure was solved and refined using the Bruker SHELXTL[33] (version 6.14) software package, using the space group *C*2/*c* (No. 15), with $Z = 8$ for the formula unit, $C_9H_{17}NClAu$. The final anisotropic full-matrix least-squares refinement on F^2 with 130 variables converged at R1 = 1.62% for the observed data and wR2 = 4.33% for all data. The goodness of fit was 1.053. The largest peak on the final difference electron density synthesis was 1.928 e/Å^3, and the largest hole was −1.072 e/Å^3 with an RMS deviation of 0.114 e/Å^3. On the basis of the final model, the calculated density was 2.086 g/cm^3 and $F(000)$ was 1392 e.

Computational Details. Møller−Plesset second-order perturbation theory (MP2)[34] was used as the primary method to calculate optimized structures, frequencies, and energetics of the ground and triplet excited states of $[Au(CO)Cl]_n$ (where $n = 1-3$). To better characterize the frequencies of the C−O stretch upon complexation, coupled-cluster theory with single, double, and quasiperturbative triple excitations (CCSD(T))[35,36] was also used. Throughout this study, the correlation consistent basis sets (cc-pV*x*Z, where x = D(2), T(3), Q(4), 5)[37] were used for C and O, while for Cl, the tight-d augmented correlation consistent basis sets (cc-pV(x+d)Z)[38] were used. For Au, the newly developed correlation consistent basis sets (cc-pV*x*Z-PP) were used,[39] which include a 60-electron Stuttgart relativistic pseudopotential.[40] The calculated absorption energies of the monomer and dimer were determined as the vertical transitions between the minimum singlet ground state S_0 and the T_1 triplet excited state (at the optimized S_0 geometry). In addition, time-dependent density functional theory (TD-DFT) calculations with B3PW91[41,42] were performed at the triple-ζ level to assess other possible excitations that contribute to the absorption spectra. The emission energies were computed from the optimized T_1 electronic state geometry and the S_0 state (at the optimized T_1 geometry). The dissociation energy (D_e) values for the dimer and trimer S_0 electronic states were predicted relative to dissociated complexes, either by calculating the energy difference between the optimized oligomer and the optimized monomers or by increasing the separation between the monomeric complexes in the optimized oligomer structure to ∼10 Å; the two methods agreed within 0.0026 eV (21 cm^{-1}) for the dimer ground state. The latter method was, therefore, adopted to estimate the excimer D_e value. All of these computations were performed with the Gaussian 03 software package,[43] except for CCSD(T) calculations, which were done using MOLPRO.[44]

Results and Discussion

1. Photophysics and Bonding in Au(CO)Cl. 1.1. Solution Absorption. The absorption spectrum of Au(CO)Cl in acetonitrile displays bands at λ_{max} 195, 207, 219, and 280 nm, as shown in Figure 1. The extinction coefficients for all these bands are concentration dependent, deviating from Beer's law. The strong absorption bands at 195, 207, and 219 nm exhibit a negative deviation from Beer's law (Table 1), while the weak

(33) *APEX2 Software Suite, Version 2.0-2*; Bruker AXS Inc., Madison, WI, 2005.
(34) Møller, C.; Plesset, M. S. *Phys. Rev. B* **1934**, *46*, 618.
(35) Purvis, G. D. I.; Bartlett, R. J. *J. Chem. Phys.* **1982**, *76*, 1910.
(36) Raghavachari, K.; Trucks, G. W.; Pople, J. A.; Head-Gordon, M. *Chem. Phys. Lett.* **1989**, *157*, 479.
(37) Dunning, T. H., Jr. *J. Chem. Phys.* **1989**, *90*, 1007.
(38) Dunning, T. H., Jr.; Peterson, K. A.; Wilson, A. K. *J. Chem. Phys.* **2001**, *114*, 9244.
(39) Peterson, K. A.; Puzzarini, C. *Theor. Chem. Acc.* **2005**, *114*, 283.
(40) Figgen, D.; Rauhut, G.; Dolg, M.; Stoll, H. *Chem. Phys.* **2005**, *311*, 227.
(41) Becke, A. D. *J. Chem. Phys.* **1993**, *98*, 5648.
(42) Perdew, J. P.; Chevary, J. A.; Vosko, S. H.; Jackson, K. A.; Pederson, M. R. *Phys. Rev. B* **1992**, *46*, 6671.
(43) Frisch, M. J.; Trucks, G. W.; Schlegel, H. B.; Scuseria, G. E.; Robb, M. A.; Cheeseman, J. R.; Montgomery, J. A., Jr.; Vreven, T.; Kudin, K. N.; Burant, J. C.; Millam, J. M.; Iyengar, S. S.; Tomasi, J.; Barone, V.; Mennucci, B.; Cossi, M.; Scalmani, G.; Rega, N.; Petersson, G. A.; Nakatsuji, H.; Hada, M.; Ehara, M.; Toyota, K.; Fukuda, R.; Hasegawa, J.; Ishida, M.; Nakajima, T.; Honda, Y.; Kitao, O.; Nakai, H.; Klene, M.; Li, X.; Knox, J. E.; Hratchian, H. P.; Cross, J. B.; Bakken, V.; Adamo, C.; Jaramillo, J.; Gomperts, R.; Stratmann, R. E.; Yazyev, O.; Austin, A. J.; Cammi, R.; Pomelli, C.; Ochterski, J. W.; Ayala, P. Y.; Morokuma, K.; Voth, G. A.; Salvador, P.; Dannenberg, J. J.; Zakrzewski, V. G.; Dapprich, S.; Daniels, A. D.; Strain, M. C.; Farkas, O.; Malick, D. K.; Rabuck, A. D.; Raghavachari, K.; Foresman, J. B.; Ortiz, J. V.; Cui, Q.; Baboul, A. G.; Clifford, S.; Cioslowski, J.; Stefanov, B. B.; Liu, G.; Liashenko, A.; Piskorz, P.; Komaromi, I.; Martin, R. L.; Fox, D. J.; Keith, T.; Al-Laham, M. A.; Peng, C. Y.; Nanayakkara, A.; Challacombe, M.; Gill, P. M. W.; Johnson, B.; Chen, W.; Wong, M. W.; Gonzalez, C.; Pople, J. A. *Gaussian 03*, revision C.02; Gaussian, Inc.: Wallingford, CT, 2004.
(44) Amos, R. D.; Bernhardsson, A.; Berning, A.; Celani, P.; Cooper, D. L.; Deegan, M. J. O.; Dobbyn, A. J.; Eckert, F.; Hampel, C.; Hetzer, G.; Knowles, P. J.; Korona, T.; Lindh, R.; Lloyd, A. W.; McNicholas, S. J.; Manby, F. R.; Meyer, W.; Mura, M. E.; Nicklass, A.; Palmieri, P.; Pitzer, R.; Rauhut, G.; Schütz, M.; Schumann, U.; Stoll, H.; Stone, A. J.; Tarroni, R.; Thorsteinsson, T.; Werner, H.-J. *MOLPRO, A Package of Ab Initio Programs Designed by H. -J. Werner and P. J. Knowles.*

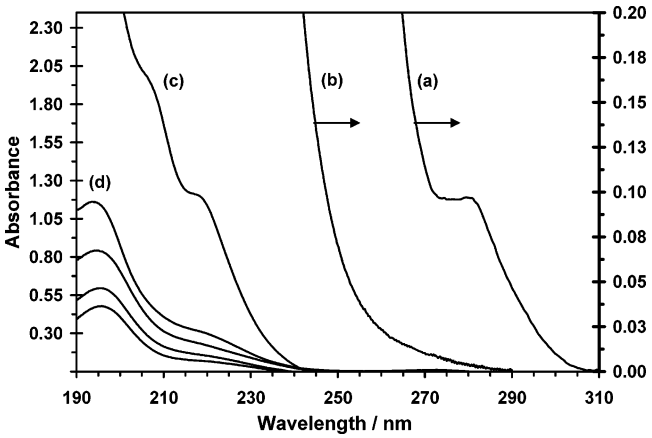

Figure 1. Absorption spectra for solutions of Au(CO)Cl in acetonitrile at various concentrations: (a) 2.56×10^{-3} M; (b, c) 5.10×10^{-4} M; (d, top to bottom, respectively) 5.10×10^{-5}, 2.56×10^{-5}, 1.27×10^{-5}, and 6.30×10^{-6} M.

Table 1. Concentration-Dependent Absorption Data for Au(CO)Cl in Acetonitrile Solutions at Ambient Temperature

	ϵ, M^{-1} cm^{-1}			
c_0, M	ϵ_{195}	ϵ_{207}	ϵ_{219}	ϵ_{280}
6.30×10^{-6}	7.52×10^4	3.17×10^4	1.84×10^4	undetectable
1.27×10^{-5}	4.68×10^4	2.15×10^4	1.27×10^4	undetectable
2.56×10^{-5}	3.28×10^4	1.53×10^4	8.75×10^3	undetectable
5.10×10^{-5}	2.27×10^4	8.69×10^3	6.27×10^3	undetectable
5.10×10^{-4}	opaque	3.96×10^3	2.51×10^3	7.84
2.56×10^{-3}	opaque	opaque	opaque	34.1
1.74×10^{-4} [a]		4.9×10^3 [a]	3.3×10^3 [a]	

[a] From ref 24 with extinction coefficients quoted at 208 and 220 nm.

peak near 280 nm appears only at high concentrations and exhibits a positive deviation from Beer's law. These data suggest the oligomerization of Au(CO)Cl complexes in solution, for which aurophilic bonding is at least one contributing factor in addition to other possible intermolecular forces such as multipolar interactions.[45] Precedents for oligomerization of Au^I complexes in solution are known, which include work by Lin and co-workers for diphosphinedithiolate dinuclear complexes[46] and Patterson and co-workers for dicyano complexes.[47] The high extinction coefficient and negative deviation from Beer's law for the major absorption bands of Au(CO)Cl at 195, 207, and 219 nm in acetonitrile are consistent with charge-transfer transitions characteristic of monomeric complexes. In contrast to the absorbance bands attributed to the monomer, a number of factors suggest that the weak band at 280 nm should be assigned to an oligomeric species such as a $[Au(CO)Cl]_2$ dimer; these factors include the low extinction coefficient known for such weakly bound aggregates,[46,47] the red shift in energy compared to the two aforementioned monomer bands, and the positive deviation from Beer's law.

1.2. Temperature-Dependent Solid-State Luminescence. Figure 2 shows the luminescence spectra for a crystalline solid of Au(CO)Cl versus temperature. The room-temperature spectrum gives rise to a broad unstructured emission with a peak in the red region and an unresolved shoulder in the orange region. The latter can be resolved from the red emission at low temperatures. The emission maxima at 295 and 77 K occur at

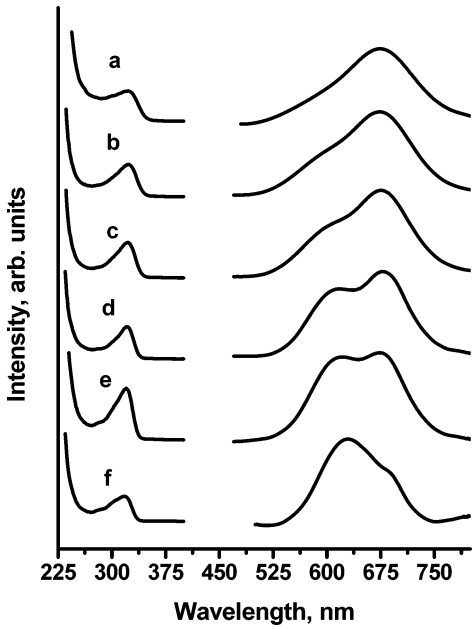

Figure 2. Photoluminescence excitation (left) and emission (right) spectra of crystals of Au(CO)Cl at various temperatures: (a) 295 K; (b) 235 K; (c) 180 K; (d) 135 K; (e) 100 K; (f) 77 K. The spectra at different temperatures are offset for the sake of clarity.

670 and 630 nm, respectively. The changes are quite progressive with temperature, as the two peaks become nearly identical in intensity around 100 K. The emission color change from red at room temperature to orange at cryogenic temperatures amounts to a modest case of "luminescence thermochromism" resulting from changes in the relative intensities of two emission bands. This is reminiscent of prior occurrences of this phenomenon in other monovalent coinage metal complexes, as are most well-known for tetranuclear $[Cu(halide)(arylamine)]_4$ clusters.[48] The two emission bands of the Au(CO)Cl solid exhibit essentially indistinguishable excitation profiles (Figure 2). Lifetimes of 28.7 $\pm$ 2.0 and 9.80 $\pm$ 0.16 μs are obtained (seemingly counterintuitive) for the peak maxima at 295 and 77 K, respectively. The decrease in the lifetime upon cooling from room temperature to 77 K is due to the fact that the peak maximum at each temperature represents an emitting state different from that at the other temperature. Biexponential fits were used to extract the lifetime of the minor component at selected temperatures in the 77−295 K range and revealed that the lifetime of each component followed the expected trend vs temperature, such that longer lifetimes were obtained upon cooling due to annihilation of the nonradiative decay rate. These results indicate that the luminescence thermochromism in Au(CO)Cl occurs as a result of relaxation (internal conversion) between two phosphorescent states, as opposed to being due to thermal compression of M···M distances, which is known for other closed-shell coordination compounds that contain M···M packing in the solid state.[49,50] The assignment is as such because thermal contraction usually leads to *gradual* shifts in the excitation and emission energies vs temperature,[50] which is different from the behavior seen for Au(CO)Cl, as well as other literature precedents (e.g., ref 49), wherein the changes are due to relaxation between two

(45) Liau, R.-Y.; Mathieson, T.; Schier, A.; Berger, R. J.; Runeberg, N.; Schmidbaur, H. *Z. Naturforsch., B* **2002**, *57*, 881.
(46) Tang, S. S.; Chang, C. P.; Lin, I. J. B.; Liou, L. S.; Wang, J. C. *Inorg. Chem.* **1997**, *36*, 2294.
(47) Rawashdeh-Omary, M. A.; Omary, M. A.; Patterson, H. H. *J. Am. Chem. Soc.* **2000**, *122*, 10371.
(48) See, for example: (a) Ryu, C. K.; Kyle, K. R.; Ford, P. C. *Inorg. Chem.* **1991**, *30*, 3982. (b) Lindsay, E.; Ford, P. C. *Inorg. Chim. Acta* **1996**, *242*, 51. (c) Ford, P. C.; Cariati, E.; Bourassa, J. *Chem. Rev.* **1999**, *99*, 3625.
(49) Dias, H. V. R.; Diyabalanage, H. V. K.; Eldabaja, M. G.; Elbjeirami, O.; Rawashdeh-Omary, M. A.; Omary, M. A. *J. Am. Chem. Soc.* **2005**, *127*, 7489.

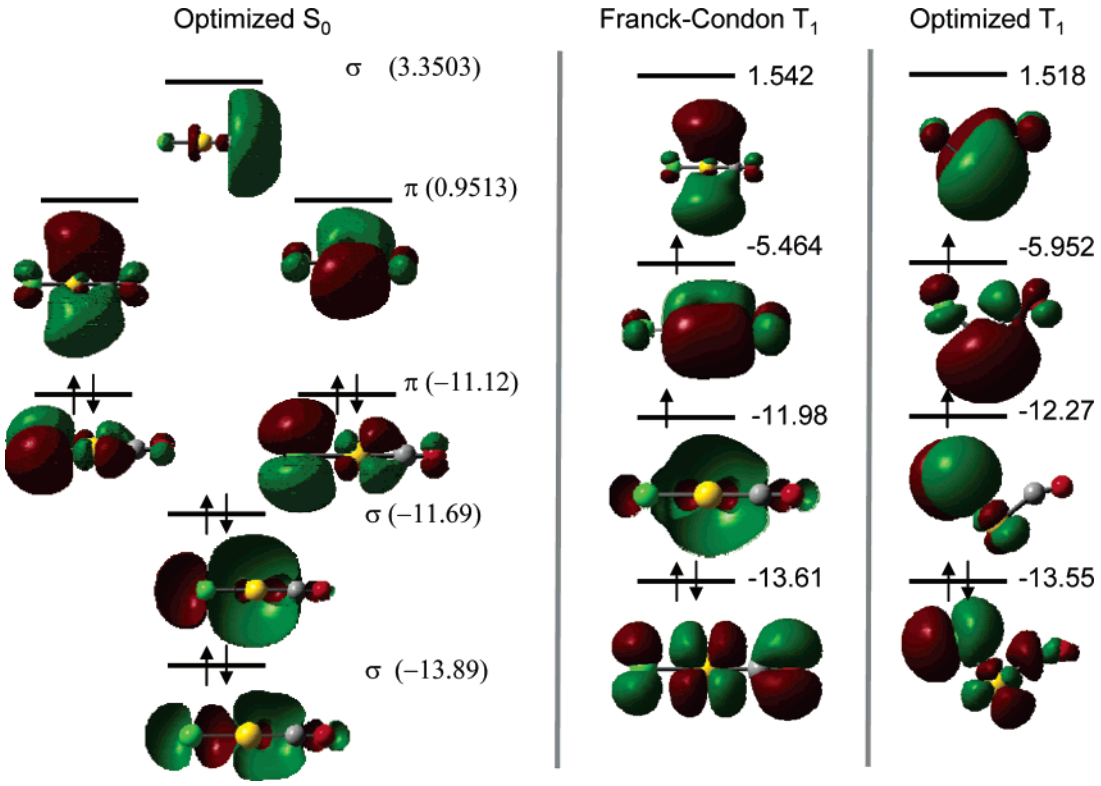

Figure 3. Hartree−Fock contours for frontier molecular orbitals of the Au(CO)Cl monomer at its optimized S_0 ground state (left), Franck−Condon vertical T_1 excited state at the S_0 geometry (middle), and fully optimized T_1 excited state (right). The data are based on the output files of MP2 calculations with the following basis sets: cc-pVDZ for Au, cc-pVDZ for CO, and cc-pV(D+d)Z for Cl. Orbital energies shown are in eV.

emitting states such that one band increases in intensity while another decreases. Analysis of the changes in the relative intensities of the two peaks in the 77−180 K temperature range (relative peak areas from a two-Gaussian fit at each temperature) gives rise to an activation energy of 170 cm^{-1} for the internal conversion from the orange-emitting state to the red-emitting state. Due to the small energy difference between the two emission peaks (<1000 cm^{-1}) and the microsecond lifetimes for each, we hypothesize that the red and orange emissions represent spin−orbit states correlating to the same T_1 triplet state, although two closely spaced triplets (T_1 and T_2) could not be ruled out. The large energy difference between the ^3D_J levels (15 040, 17 640, and 27 760 cm^{-1} for $J = 3-1$, respectively)[51] of free Au(I) due to large spin−orbit coupling ($\xi_{5d} \approx 5100$ cm^{-1})[52] makes it reasonable to make the aforementioned hypothesis that two spin−orbit states may be responsible for the red and orange emission peaks of the Au(CO)Cl solid.

1.3. Assignments of the Electronic Transitions. In an effort to shed more light on the exact orbital nature involved in the electronic transitions for Au(CO)Cl in solution and in the solid state, we have carried out a series of ab initio and DFT calculations. These calculations attempt to model the changes in the electronic absorption and emission transitions due to the ground-state aurophilic bonding and excited-state excimeric bonding by comparing the contours of the orbitals involved as well as the transition energies in monomeric and dimeric models.

Figures 3 and 4 show the Hartree−Fock contours for selected frontier molecular orbitals from MP2 calculations for the Au(CO)Cl monomer and the $[Au(CO)Cl]_2$ antiparallel dimer, respectively, in their optimized singlet ground state (S_0), Franck−Condon vertical T_1 excited-state at the S_0 geometry, and the fully optimized T_1 state. For the dimer in Figure 4, we note that the contour of the lowest unoccupied molecular orbital (LUMO) in the optimized S_0 state is not necessarily the same as that of the higher singly occupied molecular orbital (SOMO) of the T_1 states. Despite the extensive use of HOMO and LUMO contours in the literature to make conclusions about absorption and emission assignments, this use remains fundamentally inaccurate. Rather, it is more appropriate to draw conclusions about the assignment of the lowest energy excitation bands on the basis of the contours of the SOMOs of the Franck−Condon excited state and conceive the emission bands from the optimized excited states, instead of basing them on the HOMO and LUMO of the ground state. In Figure 4, for example, the ground-state S_0 LUMO contour suggests that an Au−Au π-bonded excimer may form, while an Au−Au σ-bonded excimer is actually suggested on the basis of the contour of the higher SOMO of either the Franck−Condon T_1 state involved in the excitation process or the optimized T_1 state involved in the phosphorescence process. Hence, we assign the lowest energy phosphorescence and excitation bands in the antiparallel dimer to a Au−Au σ-bonded excimer. The assignment of the luminescence bands to excimeric Au−Au bonding is consistent with the experimental spectral data in Figure 1, because the unstructured profile of the phosphorescence bands and the huge

(50) See, for example: (a) Gliemann, G.; Yersin, H. *Struct. Bonding* **1985**, *62*, 87. (b) Connick, W. B.; Henling, L. M.; Marsh, R. E.; Gray, H. B. *Inorg. Chem.* **1996**, *35*, 6261. (c) Nagasundaram, N.; Roper, G.; Biscoe, J.; Chai, J. W.; Patterson, H. H.; Blom, N.; Ludi, A. *Inorg. Chem.* **1986**, *25*, 2947. (d) Burini, A.; Bravi, R.; Fackler, J. P., Jr.; Galassi, R.; Grant, T. A.; Omary, M. A.; Pietroni, B. R.; Staples, R. J. *Inorg. Chem.* **2000**, *39*, 3158.

(51) Moore, C. E. *Atomic Energy Levels, Vol. III*; United States Department of Commerce/National Bureau of Standards: Washington, DC, 1958.

(52) Griffith, J. S. *Theory of Transition Metal Ions*; Cambridge University Press: Cambridge, U.K., 1964.

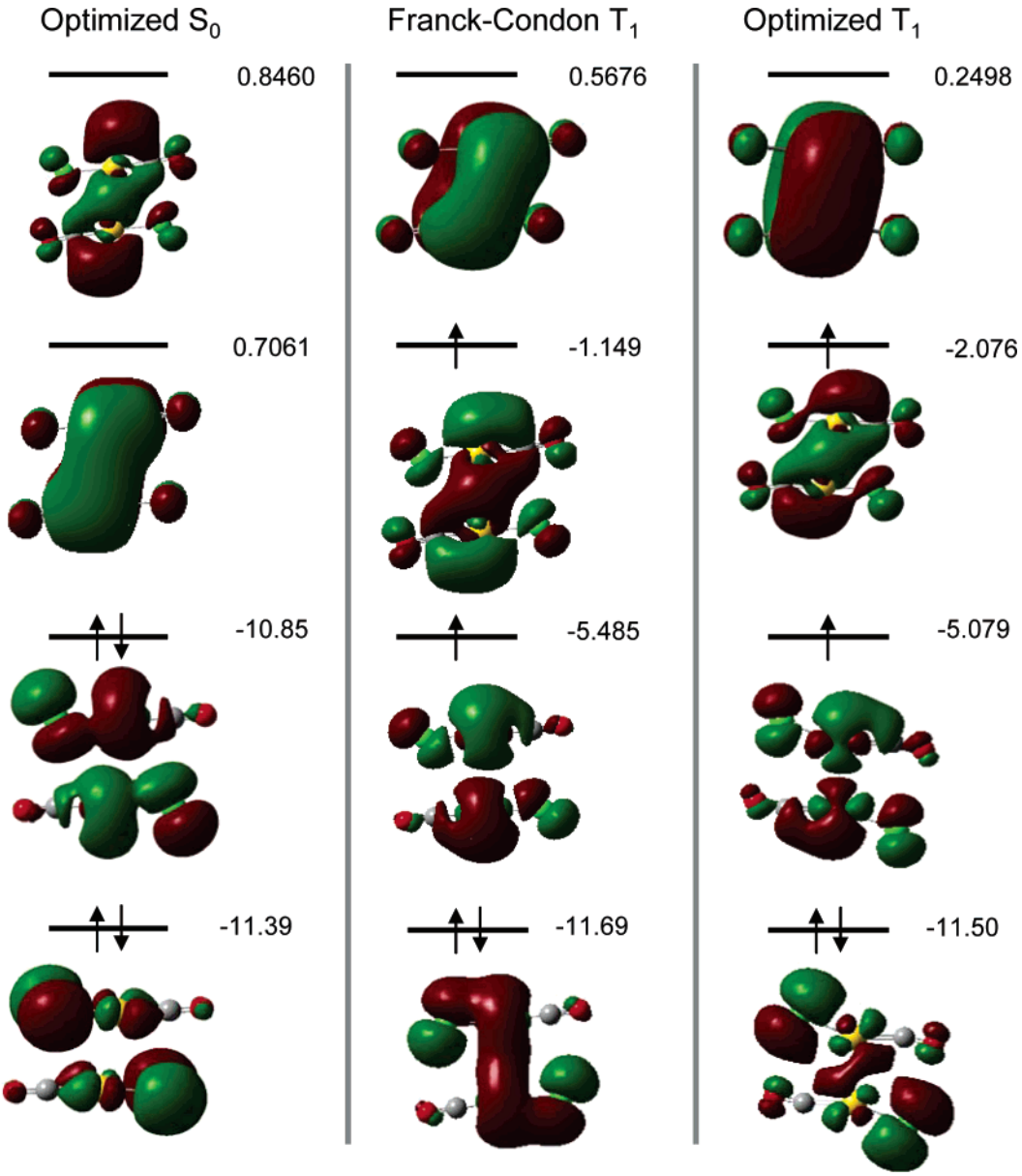

Figure 4. Restricted open-shell Hartree−Fock contours for frontier molecular orbitals from calculations for the $[(CO)AuCl]_2$ antiparallel dimer (with Cl−Au−CO at the top and OC−Au−Cl at the bottom). The contours are shown for the S_0 ground state (left), the Franck−Condon vertical T_1 excited state at the S_0 geometry (middle), and the fully optimized T_1 state (right). The methods and basis sets are the same as those in Figure 3. Orbital energies shown are in eV.

Stokes shift are typical signatures of metal-centered excimeric phosphorescence in d^{10} systems.[25,26] A recent study by Coppens, Omary, and co-workers has verified such an assignment for a trinuclear Cu(I) pyrazolate complex by pump−probe time-resolved single-crystal X-ray diffraction, in which a startling intermolecular motion was observed in the crystal structure of the excimeric phosphorescent state manifested by compressions of Cu···Cu distances and interplanar separations between adjacent trimers by 0.56 and 0.65 Å, respectively![53] Kunkely and Vogler noted that the huge Stokes shift in the Au(CO)Cl solid was indicative of large structural changes associated with electronic excitation, but they suggested that the emission was a "d−s transition" localized on the Au atom, which leads to the population of a σ^* orbital in a monomeric complex.[24] These authors also stated that "the emission may be slightly modified by Au−Au interaction". However, the additional experimental and computational data herein allow us to conclude that the emission is instead *caused* by the intermolecular Au−Au excimeric covalent bonding in the phosphorescent state, despite the weakness of the metallophilic Au···Au interaction in the ground state.

Figure 3 revisits the electronic structure of the Au(CO)Cl monomer, including the assignment of the low-lying possible electronic absorption and emission transitions. The ground-state HOMO and other low-lying occupied orbitals show the highest electron density on the Cl−Au "left" side of the Cl−Au−CO molecule, particularly on the chlorine atom. This is hardly surprising, since the chloride is conventionally classified as a π−donor ligand. Indeed, the π interactions with the chloride destabilize the Au d_π orbitals such that they become the HOMO instead of the strongly antibonding d_{z^2} ligand-field σ^* orbital, which is the HOMO-1 according to Figure 3. In contrast, the frontier virtual orbitals, which are the likely targets to be

(53) Vorontsov, I. I.; Kovalevsky, A. Yu.; Chen, Y.-S.; Graber, T.; Novozhilova, I. V.; Omary, M. A.; Coppens, P. *Phys. Rev. Lett.* **2005**, *94*, 193003.

Table 2. MP2-Calculated Geometries for the Optimized S_0 and T_1 States of $[(CO)AuCl]_n$ ($n = 1-3$ with Antiparallel Isomers for $n = 2, 3$)[a]

		bond length				bond angle	
state	basis set *x*	Cl−Au	Au−C	C−O	Au−Au	Cl−Au−C	Au−C−O
				Au(CO)Cl			
S_0	D	2.22	1.82	1.15			
	T	2.20	1.85	1.14			
T_1	D	2.34	1.94	1.16			
	T	2.31	1.93	1.15			
				$[Au(CO)Cl]_2$			
S_0	D	2.23	1.87	1.15	3.20	177.0	177.8
	T	2.22	1.86	1.14	3.17	177.1	177.9
T_1	D	2.24	1.92	1.16	2.62	158.3	166.7
	T	2.22	1.90	1.15	2.61	160.3	167.7
				$[(CO)AuCl]_3$			
S_0	D	2.23	1.87	1.15	3.13	179.5	180.0
exptl[b]							
S_0		2.26	1.93	1.11	3.38	180.0	180.0

[a] The basis set combinations are cc-pV*x*Z for C and O, cc-pV(*x*+d)Z for Cl, and cc-pV*n*Z-PP for Au. Calculated bond lengths are in Å and bond angles in deg. [b] Reference 2.

Table 3. Selected IR Frequencies (cm^{-1}) and Dissociation Energies (eV) Calculated with MP2[a]

molecule	basis set *x*	ν(C−O)	ν(Au−Au)	D_e
CO	D	2113 (2143)		
	T	2121 (2153)		
Au(CO)Cl	D	2119 (2168)		
	T	2121 (2176)		
Au(CO)Cl*	D	2052		
	T	2027		
$[Au(CO)Cl]_2$	D	2128, 2129[b]	50	0.44
	T	2130, 2132[b]	47	0.43
$[(CO)AuCl]_2$*	D	2033, 2594[b]	153	2.49
	T	2034, 2733[b]	160	2.27
$[(CO)AuCl]_3$	D	2125, 2123,[b] 2137[c]	44, 67[b]	0.91

[a] Additional values given in parentheses were computed with CCSD(T). An asterisk indicates a molecule in its optimized T_1 excited state. [b] Symmetric and asymmetric stretches, respectively. [c] The mode at 2137 cm^{-1} is primarily from the CO on the central Au while the two others are primarily from the carbonyls on the two peripheral Au atoms.

populated in the low-energy absorption transitions, generally exhibit higher electron density on the Au−CO "right" side of the Cl−Au−CO molecule than on the "left" side. The LUMO exhibits a strong Au $6p_{x,y}$ character, where gold is engaged in π* antibonding interactions with the ligands; interestingly, the admixture with the ligands involves rather similar contributions from a CO π* ligand orbital and a Cl $3p_{x,y}$ atomic orbital. This is somewhat surprising, because CO is a better π acceptor than Cl. The aforementioned orbital description is qualitatively the same within each monomer in the dimer (Figure 4), in that the frontier orbitals show delocalized character on all atoms. The common practice in the literature is to assign electronic transitions on the basis of the major compositions of the molecular orbitals allegedly involved in the electronic transitions. Thus, utilizing the data in Figures 3 and 4 suggests that the lowest energy excitation bands in Au(CO)Cl are essentially due to halide-to-metal charge transfer (XMCT) transitions from filled orbitals with a strong chloride $3p_{x,y}$ character to vacant orbitals with a strong gold $6p_{x,y}$ character. Clearly, chemical intuition alone cannot be followed for the assignment of the lowest energy absorption bands in this molecule, because one would expect an opposite assignment (i.e., metal to ligand charge transfer or MLCT) from a gold 5d filled orbital to a carbonyl π* vacant orbital. Indeed, the latter assignment has been commonly suggested in the literature for Au(CO)Cl in comparison with $Au(PR_3)Cl$ complexes.[9,24,54] More insights about the assignments of the electronic absorption bands in Au(CO)Cl, including association effects, are provided in the discussion of the TD-DFT results below.

To complete the qualitative description of the Au(CO)Cl electronic structure, we now discuss the issue of the monomer emission. Figure 3 shows that both the HOMO and LUMO are doubly degenerate orbitals in which Au exhibits π bonding and antibonding interactions with the CO ligand, respectively, suggesting that photon absorption renders the excited molecule Jahn−Teller unstable. Indeed, optimizing the T_1 triplet state gives rise to a drastic molecular distortion in which the molecule is no longer linear, as the C−Au−Cl angle becomes severely bent and the orbital degeneracy no longer exists (Figure 3). Due to the severe Jahn−Teller distortion, the calculated phosphorescence energy of the excited monomer lies in the near-IR region (vide infra). While interesting, this result, however, does not have a strong bearing on the luminescence properties of the compound and is not in agreement with the experimental data in this paper. It is believed that the Au-centered luminescence from the two-coordinate Au(I) compounds presented herein is observed only in the presence of the Au···Au interaction by association of monomeric molecules, which is consistent with what has been shown in previous literature.[25,26] Since the phosphorescence by this compound is exhibited in the solid state, whereby monomeric molecules pack adjacent to one another via aurophilic bonding, and since the computational data show that dimeric molecules exhibit Au−Au excimeric bond formation in the T_1 state, the monomer is not a good model for the luminescence behavior of the solid. The monomer model is, however, sufficient to describe dilute solutions of the Au(CO)Cl compound, while such solutions do not exhibit luminescence.

1.4. Ground- and Excited-State Bonding in $[Au(CO)Cl]_n$ Species. Table 2 shows the calculated geometric parameters for $[Au(CO)Cl]_n$ species ($n = 1-3$), while Table 3 shows the corresponding dissociation energies and vibrational frequencies for selected modes. The computed bond distances and angles within each linear complex in the S_0 ground state are comparable with the experimental crystal structure determined for Au(CO)Cl,[2] with slight improvements obtained with the larger triple-ζ basis sets. In Table 3, the calculated $\nu_{C\equiv O}$ frequencies have been predicted with both MP2 and CCSD(T). With CCSD(T) at the triple-ζ level, the free CO frequency changes from 2153 to 2176 cm^{-1} in the Au(CO)Cl species, which displays a slight blue shift upon complexation and provides computational evidence in line with the anomalous blue shift known experimentally for this metal carbonyl.[7] It must be noted that MP2 at the triple-ζ level is an insufficient level of theory to correctly predict this trend. In fact, previous computations using MP2 with different basis sets also did not attain this anomalous shift.[9,55] (While MP2 is not appropriate for the quantitative description of the $\nu_{C\equiv O}$ shift in the ground state, MP2 is traditionally considered an adequate level of theory to compute vibrational frequencies and is used later for the qualitative comparison of ground and excited states.)

The ground-state aurophilic bonding is accounted for in the present calculations because MP2 is known to describe metallophilic bonding.[56] Indeed, the theoretical methodology employed overdescribes this closed-shell bonding interaction, as

(54) Savas, M. M.; Mason, W. R. *Inorg. Chem.* **1987**, *26*, 301.
(55) Fortunelli, A.; Germano, G. *J. Phys. Chem. A* **2000**, *104*, 10834.
(56) For reviews, see: (a) Pyykkö, P. *Chem. Rev.* **1997**, *97*, 597. (b) Pyykkö, P. *Angew. Chem., Int. Ed.* **2004**, *43*, 4412. (c) Pyykkö, P. *Inorg. Chim. Acta* **2005**, *358*, 4113.

the calculated Au···Au aurophilic bond distances in the dimer and trimer (~3.13−3.20 Å, as shown in Table 2) are shorter than the crystallographic value of 3.38 Å.[2] This is partly due to inherent limitations in the MP2 method; see ref 57 for a detailed discussion of the limitations of various methods and basis sets for the description of metallophilic bonding. The D_e value for the S_0 states of the dimer and trimer, as shown in Table 3, of ~0.45 eV per bond (~10 kcal/mol) suggests aurophilic bonding in the ground state. This value is commensurate with the typical values reported for aurophilic bonds in the literature.[56] The trimer D_e value for two aurophilic bonds is slightly higher than twice the dimer D_e value, suggesting a small degree of cooperativity. Table 3 also shows that aurophilic association in the antiparallel linear oligomers leads to a ν_{Au-Au} frequency of 50 cm^{-1} in the dimer and two frequencies in the trimer of 44 and 67 cm^{-1}, representing symmetric and asymmetric Au−Au−Au stretching, respectively. When the ground-state monomer $\nu_{C\equiv O}$ frequency is compared with those of the associated dimer and trimer, the aurophilic bonded systems lead to a further blue shift of the CO frequency, as presumed since the aurophilic bonding leads to less π back-bonding to the CO (π^*), which further stabilizes the C≡O bond. On the basis of the dimer electronic structure (Figure 4) discussed above, photoexcitation leads to the formation of an excimer with a bona-fide Au−Au covalent σ bond in the relaxed geometry of the T_1 state of the dimer. This is manifested by the 2.61 Å distance calculated for this bond, representing a contraction by 0.56 Å from the ground-state aurophilic bond of the dimer (Table 2, x = T). Upon excitation to the T_1 state, the D_e value of the dimer is drastically increased by over 5 times to 2.27 eV in the resulting excimer, as shown in Table 3. The formation of this Au−Au bonded excimer also leads to drastic changes in the vibrational frequencies (Table 3). Thus, the Raman-active ν_{Au-Au} dimer frequency calculated at the MP2 triple-ζ level exhibits a drastic blue shift to 160 cm^{-1} in the optimized T_1 excimeric phosphorescent state from the 47 cm^{-1} value in the optimized S_0 aurophilic ground state. Meanwhile, the $\nu_{C\equiv O}$ frequency in the dimer S_0 ground state is centered at 2131 cm^{-1}, which becomes two well-separated bands at 2034 and 2733 cm^{-1} in the T_1 state. The average of these two $\nu_{C\equiv O}$ values (2383 cm^{-1}) is blue-shifted from the ground-state value by 252 cm^{-1}, which is likely due to the diminished π back-bonding to CO in the excimeric state caused by the now chemically bonded Au−Au centers. This is further supported by a Au−C bond (by ~0.05 Å) that is longer in the T_1 excimer than in the S_0 state dimer, which is also consistent with a weaker π back-bonding in the excimer.

1.5. Quantitative Evaluation of Photophysical Parameters. This section discusses the quantum-mechanical calculation of the electronic absorption and luminescence transitions for monomer and dimer models in relation to the experimental values. For the electronic absorption, TD-DFT is used because of the convenience of this method to compute multiple spectral transitions. The computed results are listed in Table 4 and can be compared to the experimental solution absorption data in Figure 2. The monomer TD-DFT calculations give rise to three lowest energy absorption bands with nonzero (≥0.01) oscillator strengths at 198, 227, and 240 nm, all clearly within the bands seen experimentally for dilute solutions of Au(CO)Cl in acetonitrile (Figure 2). The TD-DFT calculations further predict two lowest energy absorption bands for the dimer at 251 and 265 nm, clearly red-shifted from the monomer absorption bands, consistent with the experimental finding that increasing the concentration of Au(CO)Cl leads to the appearance of bands at energies lower than those in dilute solutions. Although the dimer absorptions are not as greatly shifted from the monomer bands as is seen experimentally, they do demonstrate that aurophilic bonding leads to a shift in the absorption spectra. It is likely that the computed smaller-than-expected red shift upon dimerization is a result of the known limitation of density functional theory in describing dispersion forces, which are significant in metallophilic bonding.[57] Overall, the computed absorption spectra for the monomer and dimer are in reasonable agreement with the experimental absorption spectra, particularly because our theoretical treatment does not include spin−orbit coupling.

For the luminescence emission and excitation transitions, we only modeled the lowest spin-forbidden transitions, since phosphorescence usually occurs from the lowest triplet (T_1) excited state. Table 4 shows the computed photophysical parameters for monomer and dimer models. The near-IR emissions of the monomer are not comparable to experiment, because monomers are not good models for describing the Au-centered emissions in two-coordinate Au(I) complexes (vide supra), as discussed earlier. As for the dimer, the MP2-calculated phosphorescence energy lies in the violet region near 400 nm with both basis set levels used, while the experimental solid-state emission is in the red region. Although the calculated Stokes shift is similar in magnitude to that experimentally determined for the solid and is consistent with the drastic excited-state distortion in the excimeric state, the discrepancy between the calculated violet $T_1 \rightarrow S_0$ excimer emission and the red phosphorescence of solid Au(CO)Cl renders the dimer model insufficient to describe the species responsible for the solid-state emission. Given this discrepancy, we decided to explore the hypothesis that the solid-state emission is caused by an excited-state oligomer that is larger than a dimer due to delocalized Au−Au excimeric bonding beyond two adjacent units. Because modeling trimers and larger clusters with MP2 is rather demanding computationally, the problem proved easier to solve experimentally. Hence, we have carried out photoluminescence studies for 77 K frozen solutions of Au(CO)Cl at different concentrations in CH_2Cl_2 (which was chosen due to solubility reasons, although it does not form a transparent glass at 77 K, like 2-MeTHF or EPA). Figure 5 shows the results of these studies versus concentration. Frozen solutions of Au(CO)Cl in dichloromethane exhibit strong luminescence, even with concentrations as low as 5×10^{-5} M, at which the dominant band maximum is at 410 nm along with a small shoulder around 560 nm, as shown in Figure 5. The longer wavelength peak is due to larger oligomers that have an aggregation number close to that of the luminescent species in the solid state, while the shorter wavelength peak is due to a smaller oligomer, possibly a dimer. A further increase in the concentration leads to a corresponding increase in the relative intensity of the longer wavelength band, which is red-shifted to 590 nm, as it becomes the most pronounced emission band at 0.05 M. This red shift is attributed to the formation of larger oligomers as the solution concentration increases. The position of the shorter wavelength band is unaffected by concentration. Our study clearly shows the presence of two types of oligomers in frozen solutions of Au(CO)Cl in dichloromethane and suggests the increasing tendency for the formation of larger oligomers upon increasing the concentration. Lifetime data obtained for both peaks are consistent with Au-centered phosphorescent emissions from

(57) Omary, M. A.; Sinha, P.; Bagus, P. S.; Wilson, A. K. *J. Phys. Chem. A.* **2005**, *109*, 690.

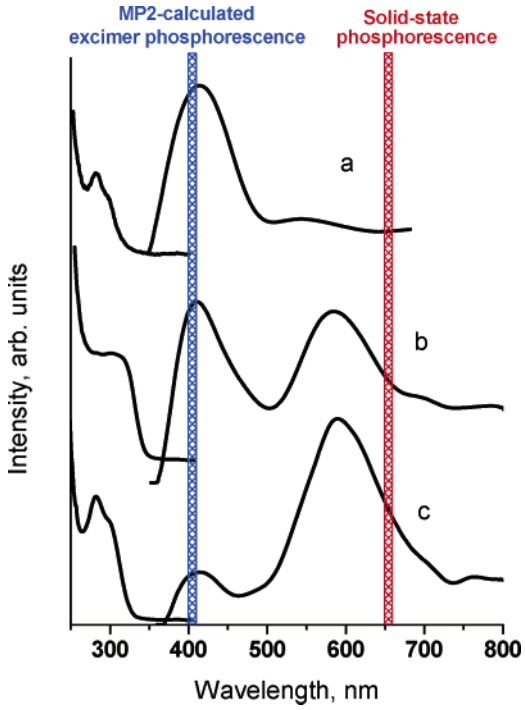

Figure 5. Photoluminescence excitation (left) and emission (right) spectra of frozen solutions (77 K) of Au(CO)Cl in CH_2Cl_2 at different concentrations: (a) 5.0×10^{-5} M; (b) 5.0×10^{-3} M; (c) 5.0×10^{-2} M.

largely distorted excited states ($\tau = 1.21 \pm 0.15$ and 7.27 ± 0.46 μs for the bands with maxima at 410 and 590 nm, respectively). Remarkably, the most dilute solutions to exhibit luminescence give rise to phosphorescence bands that lie in the same violet region as that where the MP2 calculations in Table 4 predict the excimer $T_1 \rightarrow S_0$ phosphorescence to take place. As the concentration is increased, the violet emission near 400 nm is diminished while lower energy phosphorescence bands are observed, ultimately approaching the solid-state behavior in frozen solutions with the highest concentration studied. These findings bear out the aforementioned hypothesis, because the larger oligomers in the solid state will be broken down into smaller oligomers upon dissolution, which would then emit at higher energy than in the solid state.

2. Photophysics of Linear-Chain LAuX Complexes. Neutral isonitrile compounds that have supramolecular structures similar to the that of Au(CO)Cl (i.e. antiparallel chains) have similar luminescence properties with an orange-red phosphorescent emission and an extremely large Stokes shift (~15 000−20 000 cm^{-1}), as shown in Figure 6. Stokes shifts with such large magnitudes indicate that the excited states are drastically distorted with bonding properties different from those of the ground state, as in the case for the Au(CO)Cl complex. The lifetimes at 77 K for (CyNC)AuCl, (*t*-BuNC)AuCl, and (MeNC)AuCl are 30, 40, and 79 μs, respectively. The broad/unstructured profiles and the magnitudes of the lifetime values for the emission bands of the gold isonitrile chloride and gold carbonyl chloride compounds are consistent with Au-centered phosphorescent emissions from excited states in which the Au−Au excimeric bonding is delocalized beyond two adjacent complexes. Also as in Au(CO)Cl, solutions of (RNC)AuCl in dicholromethane show no luminescence at ambient temperature but concentration-dependent studies for frozen solutions show higher energy excimeric phosphorescent emissions significantly blue-shifted from the solid-state phosphorescence. To demonstrate with a representative example, Figure 7 shows that frozen solutions of (*t*-BuNC)AuCl in dichloromethane give rise to at least three phosphorescence bands that we assign to three *[(*t*-BuNC)AuCl]$_n$ oligomers. At high concentration, the relative intensities of the three major bands are dependent on the excitation maxima (Figure 7). Upon excitation at short wavelengths, the band at 680 nm is the dominant feature, whereas the band at 420 nm becomes the dominant feature upon excitation at longer wavelength. At lower concentration, the dominant bands are those at 420 and 525 nm when using long-wavelength excitation maxima, while no peaks are observed when using short-wavelength excitation, as shown in Figure 7. Lifetime data for the three peaks are consistent with Au-centered phosphorescent emissions ($\tau = 0.97 \pm 0.12$, 2.6 ± 0.29, and 32.5 ± 1.97 μs are obtained for the bands with maxima at 420, 525, and 680 nm, respectively).

The spectral findings herein suggest that predictive information about the supramolecular structure may be obtained by the luminescence behavior. This is exemplified by crystals of (Me_4-BuNC)AuCl, whose red-orange luminescence (Figure 6) anticipated an extended-chain supramolecular structure, which was verified crystallographically at a later stage during the course of this investigation. Figure 8 shows that this compound exhibits a crystal structure in which the molecules are packed in zigzag chains with alternating short (3.418 Å) and long (4.433 Å) aurophilic distances. The crystal data for the complex are given in Table 5, while selected interatomic distances and angles for the neutral complex are given in Table 6. The Au−Cl distance is 2.253(2) Å, and the C−Au distance is 1.929(2) Å. For a comparison, the C−Au and Au−Cl distances in (CyNC)AuCl, in which molecules associate in a similar head-to-tail fashion, are 1.961(4) and 2.258(4) Å, respectively.[3] The increase in the Au−C bond length might be due to an increase in the electrostatic effects of the ligand. Each gold atom is nearly linearly coordinated by the two ligands, as indicated by the Cl−Au−C angle of 176.37(6)°, which is consistent with the

Table 4. Computed Photophysical Parameters for the Monomer and Antiparallel Dimer of Au(CO)Cl in Comparison with Experimental Data for the Solid and Frozen Solutions of Au(CO)Cl[a]

model	basis set *x*	$\lambda_{exc}(S_0 \rightarrow T_1)$ (nm)	$\lambda_{em}(T_1 \rightarrow S_0)$ (nm)	Stokes shift (10^3 cm^{-1})	$\lambda_{abs}(S_0 \rightarrow S_n)$ (nm)
Au(CO)Cl	D	220	824	33.344	
	T	220	788	32.851	197 (0.01), 227 (0.27), 240 (0.03)
$[Au(CO)Cl]_2$	D	246	407	16.088	
	T	244	394	15.573	251 (0.01), 265 (0.06)
exptl (solid)		322	674	16.200	
exptl (frozen soln)		282	412	11.200	

[a] The basis set combinations are cc-pV*x*Z for C and O, cc-pV(*x*+d)Z for Cl, and cc-pV*n*Z-PP for Au. The λ_{exc} and λ_{em} values for the spin-forbidden transitions are calculated via MP2, while the λ_{abs} values for spin-allowed transitions are calculated via TD-DFT with the oscillator strength values given in parentheses.

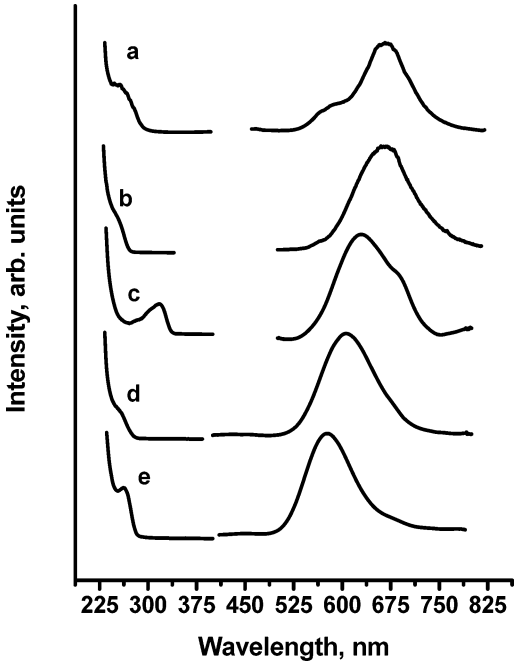

Figure 6. Photoluminescence excitation and emission spectra for crystals of (a) (Me_4BuNC)AuCl, (b) (*t*-BuNC)AuCl, (c) Au(CO)Cl, (d) (CyNC)AuCl, and (e) (MeNC)AuCl at 77 K.

analogous structure of (CyNC)AuCl, where the Cl−Au−C angle is 178.2(4)°.[3] The dihedral angles of C−Au−Au−C and Cl−Au−Au−Cl are all 180.0°. Molecules of (Me_4BuNC)AuCl self-associate to from dimers with an Au···Au distance of 3.418 Å, but these dimers pack to form extended loose chains. The neighboring Au···Au contact between adjacent dimers in the loose chain is 4.433 Å, which lies outside the accepted range of significant aurophilic bonding (2.9−3.6 Å). For comparison, crystals of (CyNC)AuX form infinite chains with alternating Au···Au contacts of 3.3894(7) and 3.5816(7) Å for X = Cl, 3.4864(9) and 3.7036(9) Å for X = Br, and 3.7182(11) and 3.9304(12) Å for X = I.[3] The head-to-tail orientation along the chains of (Me_4BuNC)AuCl molecules is favored, since the adjacent dipoles of the molecules alternates as the dipole−dipole interactions are dominant.

Although the ground-state aurophilic bonding is essentially nonexistent between adjacent dimers in crystals of (Me_4BuNC)AuCl, the luminescence properties of these crystals are distinctly different from those of dimeric species such as the lower concentrations in frozen solutions of Au(CO)Cl and (*t*-BuNC)AuCl shown in Figures 5 and 7, respectively, or single crystals of ((*p*-tosyl)CH_2NC)AuCl.[28] These species exhibit a dimeric structure and blue-green emissions with Stokes shifts significantly smaller than those observed for the crystalline solid state of infinite-chain complexes, including crystals of (Me_4BuNC)AuCl. Thus, the red-orange emission with a huge Stokes shift for (Me_4BuNC)AuCl crystals suggests the delocalization of the excimeric bonding beyond two adjacent molecules in the solid state, possibly due to cooperative M−M excimeric bonding, as suggested for other systems exhibiting this bonding.[57] For this delocalization to take place, the 4.433 Å distances in (Me_4BuNC)AuCl chains of dimers must shrink in the phosphorescent state of these crystals. While this distance is clearly too long for any significant ground-state interactions, it is not too long for excimeric interactions involving d^{10} monovalent coinage metals. A relevant comparison exists with the aforementioned time-resolved X-ray diffraction study for crystals of the trinuclear Cu(I) pyrazolate $\{[3,5\text{-}(CF_3)_2Pz]Cu\}_3$.[53] The emitting species of that system has been identified as a hexanuclear dimer- of-trimer unit, owing to intertrimer Cu−Cu contraction. Remarkably, although the ground-state Cu···Cu intertrimer separations are 3.787 and 4.018 Å, it was the longer distance that contracted in the phosphorescent state.[53] If one considers the difference in the van der Waals radii between the two metals

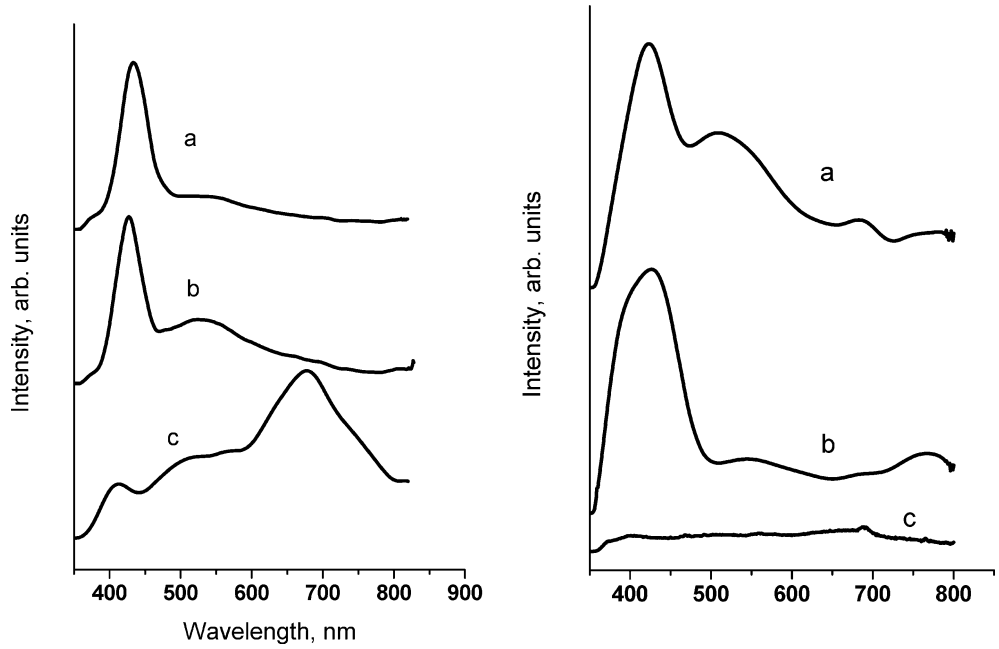

Figure 7. Photoluminescence emission spectra of frozen solutions (77 K) of (*t*-BuNC)AuCl in CH_2Cl_2 at different excitation wavelengths: (a) 335 nm; (b) 310 nm; (c) 275 nm. The spectra on the left side are for a 0.05 M solution, while the spectra on the right side are for a 5×10^{-5} M solution.

Table 5. Crystal Data for $[(CH_3)_3CCH_2C(CH_3)_2NC]AuCl$

empirical formula	$C_9H_{17}NClAu$
formula wt	371.65
temp	100(2) K
savelength	0.710 73 Å
cryst size	0.44 × 0.36 × 0.10 mm
cryst habit	clear, colorless plate
cryst syst	monoclinic
space group	*C*2/*c* (No. 15)
unit cell dimens	
a	19.9362(9) Å
b	8.0691(4) Å
c	14.8652(7) Å
α	90°
β	98.263(2)°
γ	90°
V	2366.50(19) Å^3
Z	8
density (calcd)	2.086 Mg/m^3
abs coeff	12.613 mm^{-1}
F(000)	1392

Table 6. Selected Bond Lengths (Å) and Bond Angles (deg) for the Structure of $[(CH_3)_3CCH_2C(CH_3)_2NC]AuCl$

Au1−C1	1.929(2)	Au1−Cl1	2.2532(5)
N1−C1	1.137(3)	N1−C2	1.468(3)
C2−C4	1.524(3)	C2−C3	1.529(3)
C2−C5	1.536(3)	C3−H3A	0.9800
C1−Au1−Cl1	176.37(6)	C1−N1−C2	174.9(2)
N1−C1−Au1	177.06(18)	N1−C2−C4	107.69(17)
N1−C2−C3	105.26(15)	C4−C2−C3	110.08(18)
N1−C2−C5	108.38(16)	C4−C2−C5	115.84(16)
C3−C2−C5	109.05(18)	C2−C3−H3A	109.5

(r_{vdw} = 1.40 Å for Cu^I vs r_{vdw} = 1.70 Å for Au^I),[58] the Cu^I···Cu^I separation of 4.018 Å in $\{[3,5\text{-}(CF_3)_2Pz]Cu\}_3$ is chemically similar to an analogous Au^I···Au^I separation of 4.618 Å, which is even longer than the 4.433 Å intermetal distances in chains of $(Me_4BuNC)AuCl$ complexes.

Acknowledgment. Partial support by the Robert A. Welch Foundation (Grant B-1542 to M.A.O.), the National Science Foundation (CAREER Award Grants CHE-0349313 and CHE-0239555 to M.A.O. and A.K.W., respectively), the U.S. Department of Energy (Award DE-FC26-06NT42856 to M.A.O.), and the U.S. Department of Education (P116Z050070 to A.K.W. for the Center for Advanced Scientific Computing and Modeling (CASCaM)) are gratefully acknowledged. Computational resources were provided by the NSF-CRIF (CHE-0342824) and the National Computational Science Alliance under CHE010021, which utilized the NCSA IBM p690. Additional computational support was provided by the University of North Texas Academic Computing Services.

(58) Bondi, A. *J. Phys. Chem.* **1964**, *68*, 441.

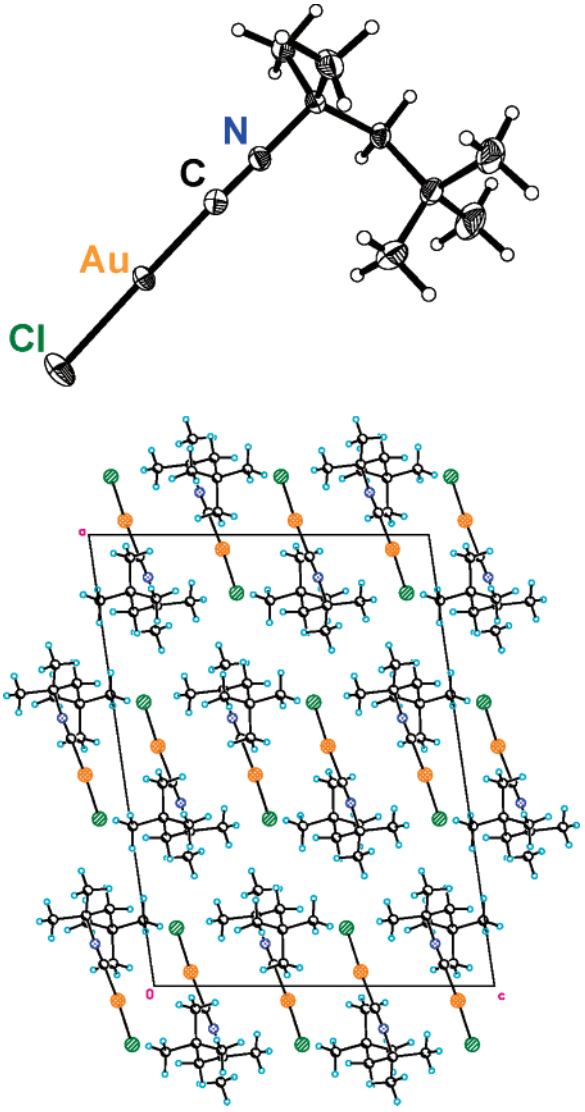

Figure 8. Crystal structure of $[(CH_3)_3CCH_2C(CH_3)_2NC]AuCl$. The top figure shows anisotropic atomic displacement ellipsoids for the non-hydrogen atoms at the 50% probability level, while hydrogen atoms are displayed with an arbitrarily small radius. The bottom figure shows the molecular packing with the view showing the projection down the *b* axis.

Supporting Information Available: CIF file giving X-ray crystallographic data for $[(CH_3)_3CCH_2C(CH_3)_2NC]AuCl$. This material is available free of charge via the Internet at http://pubs.acs.org.

OM060524T